# Oxygen Atom Abstraction of Hydrogen Chemisorbed on a Silicon Surface

**J. Ree**

*Department of Chemistry Education, Chonnam National University, Kwangju, Korea*

**Y. H. Kim**

*Department of Chemistry and Center for Chemical Dynamics, Inha University, Inchon, Korea*

**H. K. Shin***

*Department of Chemistry, University of Nevada, Reno, Nevada 89557*

*Received: February 19, 2003*

We have calculated the probability of OH (OD) formation and energy deposit of the reaction exothermicity in the newly formed OH (OD), particularly in its vibrational motion, in the gas-surface reactions O(g) + H(ad)/Si → OH(g) + Si and O(g) + D(ad)/Si → OD(g) + Si. The reaction probabilities are about 0.10 at gas temperature 1500 K and surface temperature 300 K. The vibrational and translational motions of product OH share most of the reaction energy. Increasing the initial vibrational state of the adsorbate from the ground state to $v = 1$, 2, and 3 causes the vibrational energy of OH (OD) to rise nearly linearly, whereas the energies shared by other motions vary only slightly. The product vibrational excitation is strong in both OH and OD, leading to a population inversion. The amount of energy propagated into the bulk solid phase is about 13 % of the reaction energy in the O(g) + H(ad)/Si reaction, but the amount is significantly lower in O(g) + D(ad)/Si. The dependence of reaction probabilities and energy distributions on surface temperature is found to be weak, in the range of 0−600 K.

## I. Introduction

In gas−adatom interactions taking place on a solid surface, important reactive events involve the dissociation of the adatom−surface bond and association of the gas atom with the desorbing adatom. Such reactions are often highly exothermic, so a large amount of energy is deposited in the various motions of the product state. For example, chemisorption energies of atoms such as hydrogen and oxygen on a close-packed metal surface lie in the range of 2−3 eV,[1,2] whereas the energy of the bond formed between such atoms is 4−5 eV.[3] Thus, the reaction exothermicity is nearly 2 eV, which is to be distributed among various motions of the products, including the solid phase. An Eley−Rideal (ER) mechanism has been proposed to study such exothermic gas−surface reactions, most involving chemisorbed hydrogen atoms.[4−12] The exothermicity is still significant in the reactions involving a nonmetallic surface such as graphite or silicon.[13−17] In such reactions where the surface is covered either sparsely or completely by chemisorbed hydrogen atoms, the possible reaction pathways involve the production of diatomic or polyatomic species depending on the nature of incident particles. The characterization of time evolution of such reactive events and energy disposal in the product state is important in elucidating the mechanistic details. Furthermore, such reactions can produce active surface sites, which can subsequently react with incident or preadsorbed molecules or atoms. Although the reactions taking place on a metallic surface are important in studying catalysis, those occurring on a silicon surface are of importance in the processing of silicon-based materials.

In the present paper, we study oxygen atom abstraction of hydrogen chemisorbed on a silicon surface, O(g) + H(ad)/Si → OH(g) + Si with particular emphasis on disposal of the reaction exothermicity in the vibrational motion of OH for a range of initial excitations of the adatom−surface vibration. Pathways for the distribution of reaction exothermicity as well as energy transfer probabilities and time scales of OH formation are quantities of particular interest in the present study. We then compare the result with that of O(g) + D(ad)/Si → OD(g) + Si to study the effects of deuteration. We will use a modified version of the London−Eyring−Polanyi−Sato (LEPS) procedure, which includes additional energy terms that result from the participation of adjacent surface sites in the oxygen-to-surface interaction,[18,19] for the potential energy surface. We combine the reaction-zone equations of motion with the equations of many atoms on the surface and solve these equations[20,21] for the modified LEPS potential energy. The incorporation of surface atom dynamics enables us to determine the flow of energy between the reaction zone and solid in an accurate way. We consider the reaction to take place at a gas temperature of 1500 K and surface temperature of 300 K.

## II. Model

The model for the interaction of atomic oxygen with H (or D) chemisorbed on the Si(001)−(2 × 1) surface reconstructed by forming the dimer along the [110] direction is shown in Figure 1. The hydrogen atom is chemisorbed on the Si atom of the symmetric dimer structure. The adatom site, denoted by "Si" in Figure 1, is surrounded by eight adjacent surface-layer atoms. This atom is the first atom of the *N*-atom chain, i.e., a total of $N + 1$ atoms, and is referred to as the zeroth atom ($N = 0$) on

* To whom correspondence should be addressed. E-mail: shin@unr.nevada.edu.

10.1021/jp030227r CCC: $25.00 
Published on Web 05/31/2003

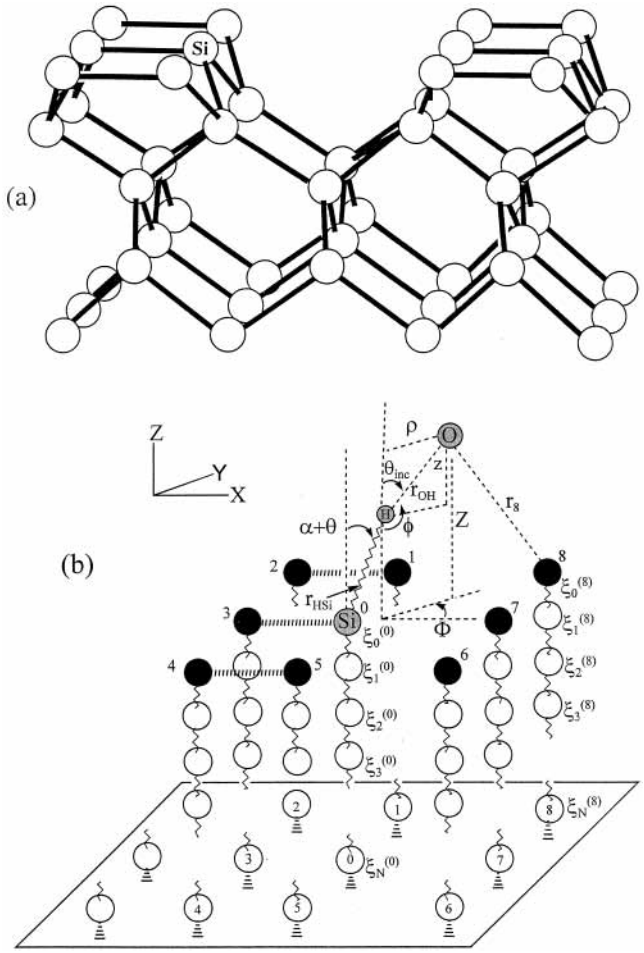


**Figure 1.** (a) Symmetric Si−Si dimer structure. Six dimers are shown in the top layer. (b) Interaction model. The zeroth Si atom on which H is chemisorbed is surrounded by eight adjacent Si atoms. The *N*-atom chain connects the H−Si vibration of the reaction zone to the heat bath. The coordinates $(r_{HSi},\theta,\phi)$ for H, $(\rho,Z,\Phi)$ for O, and $\xi$'s for the *N* chain atoms are defined. $\alpha$ is the tilt angle, $r_{OH}$ is the O to H distance, and $r_i$ is the O to the *i*th surface-layer Si distance (only $r_8$ is indicated). The zeroth and eighth chains, denoted by the vibrational coordinates $\xi_i^{(0)}$ and $\xi_i^{(8)}$ for $i = 0, 1, ..., N$, are shown.

which the hydrogen atom is chemisorbed (see Figure 1b). The incident atom also interacts with bare surface-layer atoms, which are in turn coupled to the inner atoms of each chain. The last atom of each chain, i.e., the *N*th atom, is bound to the bulk phase. Thus, the total number of Si atoms considered is $9(N + 1)$ of the zeroth, first, ..., ninth chains. The energies of all of these interactions are included in constructing the potential energy surface (PES) and used in solving the equations of motion. The incident atom, the adatom, and all of these $9(N + 1)$ Si atoms belong to the primary zone, i.e., total of $2 + 9(N + 1)$ atoms. The remaining bulk solid phase can then be referred to as the secondary zone.

When we use the coordinates defined in Figure 1, the functional dependence of distances from the gas atom to nine surface atoms have the form $r_i \equiv r_i(r_{HSi},\theta,\phi,\rho,Z,\Phi)$ and O(g)-to-H(ad) distance $r_{OH} \equiv r_{OH}(r_{HSi},\theta,\rho,Z)$. Here the index *i* signifies the first (or surface) atom of the *i*th chain. The overall interaction energy can then be denoted by $U(r_{HSi},\theta,\phi,\rho,Z,\Phi,\{\xi\})$, where $\{\xi\}$ is the collective notation for all nine chain sets for each set of vibrational coordinates consisting of $(N + 1)$ atoms $(\xi_0, \xi_1, ..., \xi_N)$. To express the interaction energy in this fashion, we have transformed the coordinates of the incident gas atom $(x_O,y_O,z_O)$ into the cylindrical system $(\rho,Z,\Phi)$ and the adatom coordinates $(x_H,y_H,z_H)$ into the natural system $(r_{HSi},\theta,\phi)$. One angle, which greatly affects the geometry of the collision system, is the inclination angle $\alpha$, which is known to be 20.6°.[22] We take the LEPS−PES for the interactions of O to H, H to the *zero*th Si, O to the *zero*th Si, and O to eight adjacent surface atoms, all of which are considered to be exponential. We then combine the LEPS function to the potential energy representing the vibrational motions of the *N*-atom chain, which is surrounded by eight additional chains as shown in Figure 1b. The chain atoms are coupled to each other through the harmonic potential energy $^1/_2M_s\omega_{ej}^2\xi_j^2$, where $M_s$ is the mass of the silicon atom and $\omega_{ej}$ is the Einstein frequency. We note that the sum of solid interaction potential energies includes cross terms such as $^1/_2M_s\omega_{cj}^2\xi_{j-1}\xi_j$, $^1/_2M_s\omega_{c,j+1}^2\xi_j\xi_{j+1}$, etc., where $\omega_{cj}$ is the coupling constant characterizing the chain. The overall potential energy, including the $\theta$ and $\phi$ terms, is given by

$$U(r_{HSi},\theta,\phi,\rho,Z,\Phi,\{\xi\}) = \{Q_{OH} + Q_{HSi} + Q_{OS} - [A_{OH}^2 + A_{HSi}^2 + A_{OS}^2 - A_{OH}A_{HSi} - (A_{OH} + A_{HSi})A_{OS}]^{1/2}\} + {}^1/_2k_\theta(\theta - \theta_e)^2 + {}^1/_2k_\phi(\phi - \phi_e)^2 + \sum_i[\sum_j({}^1/_2M_s\omega_{ej}^2\xi_j^2)_i + \sum_j(\text{terms of type } {}^1/_2M_s\omega_{cj}^2\xi_{j-1}\xi_j, {}^1/_2M_s\omega_{c,j+1}^2\xi_j\,\xi_{j+1}, \text{etc.})_i] \quad (1)$$

where $k_\theta$ and $k_\phi$ are the force constants, $\theta_e$ and $\phi_e$ are the equilibrium angles, and $i = 0-8$. Note that the hydrogen atom is chemisorbed on the zeroth Si atom of the $i = 0$ chain (see Figure 1b). The Coulombic and exchange terms are

$$Q_k = {}^1/_4[D_k/(1 + \Delta_k)][(3 + \Delta_k)e^{(r_{ke}-r_k)/a_k} - (2 + 6\Delta_k)e^{(r_{ke}-r_k)/2a_k}] \quad (2a)$$

$$A_k = {}^1/_4[D_k/(1 + \Delta_k)][(1 + 3\Delta_k)e^{(r_{ke}-r_k)/a_k} - (6 + 2\Delta_k)e^{(r_{ke}-r_k)/2a_k}] \quad (2b)$$

for $k =$ OH or HSi and $D_k$ and $a_k$ are the potential parameters. For the O−surface (OS) interaction, the energy comprises nine terms, including the contribution of the H to zeroth Si interaction

$$Q_{OS} = {}^1/_4[D_{OS}/(1 + \Delta_{OS})]\sum_{i=0}^{8}[(3 + \Delta_{OS})e^{(r_{ie}-r_i)/a_{OS}} - (2 + 6\Delta_{OS})e^{(r_{ie}-r_i)/2a_{OS}}] \quad (3a)$$

$$A_{OS} = {}^1/_4[D_{OS}/(1 + \Delta_{OS})]\sum_{i=0}^{8}[(1 + 3\Delta_{OS})e^{(r_{ie}-r_i)/a_{OS}} - (6 + 2\Delta_{OS})e^{(r_{ie}-r_i)/2a_{OS}}] \quad (3b)$$

where $r_i$ is the distance between O and first Si atom of the *i*th chain. Each Coulombic or exchange term of the LEPS potential energy contains the Sato parameter ($\Delta$). By varying their values systematically, we obtain the parameter which best describes the desired features of minimal barrier height and attractive well depth in both the entrance and exit channel to be $\Delta_{OH} = 0.50$, $\Delta_{HSi} = -0.05$, $\Delta_{OS} = 0.20$ for the oxygen-to-eight surface layer Si atom interactions, and $\Delta_{OS} = 0.50$ for the oxygen-to-adatom site. The attractive potential energy surface constructed with these parameters is shown in Figure 2, where both the fine and coarse plots are presented. In Figure 2b, we find the barrier height of 0.53 kcal/mol for O(g) + H(ad)/Si. The observed activation energies for the related systems of D(g) + H(ad)/Si

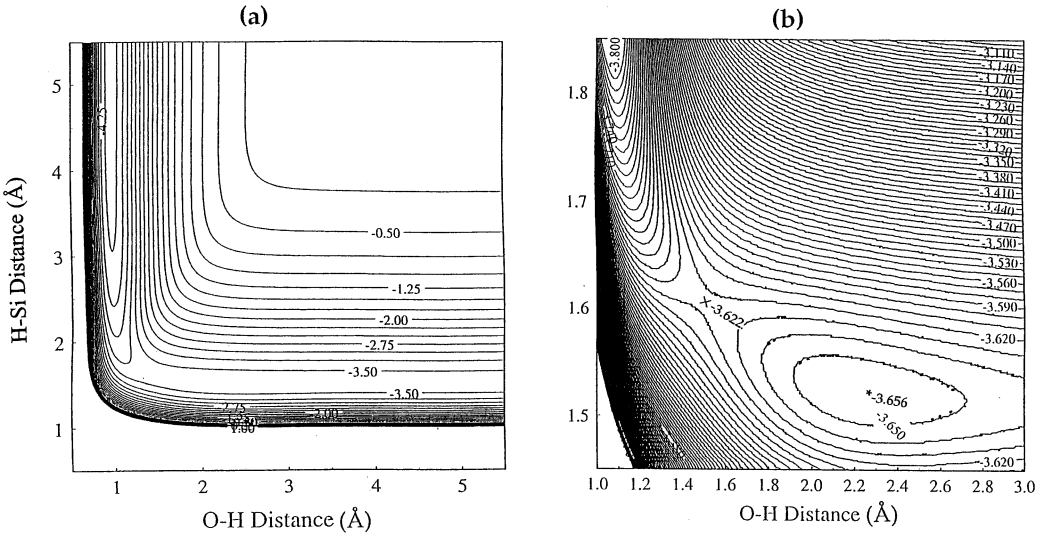


**Figure 2.** Attractive potential energy surfaces in (a) coarse scale and (b) fine scale in the direction of $\theta = \phi = \Phi = 0°$ for the $b = 0$ collision. In b, the position of the barrier is indicated by "×" at −3.622 eV. The asterisk indicates the position of the potential minimum (−3.656 eV) in the entrance channel. The labeled contours are in eV; they are in (a) 0.25 eV intervals and (b) 0.010 eV intervals.

and H(g) + D(ad)/Si are 1.06 ±0.11 and 0.55 ±0.05 kcal/mol,[13] respectively. A positive value of Δ tends to favor the formation of the indicated bond, and a negative value tends to promote the dissociation. Although the above set eliminates an attractive potential well in the product channel, it produces a very shallow well of depth of 0.25 kcal/mol in the entrance channel. Because of this well, there can be a finite but small probability of the incident atom being trapped on the surface without undergoing reaction. (We will consider this aspect in section IIIA).

To study the reactive event rigorously, we follow the time evolution of the reaction system by integrating the equations of dynamics, which describe the motions of the incident atom, adatom, and 9($N$ + 1) chain atoms. The equations of motion for the incident oxygen atom and adsorbed hydrogen atom are

$$m_O\ddot{Z}(t) = -\partial U(r_{HSi},\theta,\phi,\rho,Z,\Phi,\{\xi\})/\partial Z \quad (4a)$$

$$\mu_{OH}\ddot{\rho}(t) = -\partial U(r_{HSi},\theta,\phi,\rho,Z,\Phi,\{\xi\})/\partial \rho \quad (4b)$$

$$I_{OH}\ddot{\Phi}(t) = -\partial U(r_{HSi},\theta,\phi,\rho,Z,\Phi,\{\xi\})/\partial \Phi \quad (4c)$$

$$\mu_{HSi}\ddot{r}_{HSi}(t) = -\partial U(r_{HSi},\theta,\phi,\rho,Z,\Phi,\{\xi\})/\partial r_{HSi} \quad (4d)$$

$$I_{HSi}\ddot{\theta}(t) = -\partial U(r_{HSi},\theta,\phi,\rho,Z,\Phi,\{\xi\})/\partial \theta \quad (4e)$$

$$I_{HSi}\ddot{\phi}(t) = -\partial U(r_{HSi},\theta,\phi,\rho,Z,\Phi,\{\xi\})/\partial \phi \quad (4f)$$

where $\mu$ and $I$ are the reduced mass and moment of inertia of the diatomic species indicated. Here, $m_O$ is the mass of the oxygen atom replacing the reduced mass of collision for the relative motion, which is determined by the incident gas atom. For each ($N$ + 1)-atom chain dynamics, we have[16]

$$M_s\ddot{\xi}_0(t) = -M_s\omega_{e,0}^2\xi_0(t) + M_s\omega_{c,1}^2\xi_1(t) - \partial U(r_{HSi},\theta,\phi,\rho,Z,\Phi,\{\xi\})/\partial \xi_0 \quad (5a)$$

$$M_s\ddot{\xi}_1(t) = -M_s\omega_{e,1}^2\xi_1(t) + M_s\omega_{c,1}^2\xi_0(t) + M_s\omega_{c,2}^2\xi_2(t) \quad (5b)$$

$$M_s\ddot{\xi}_0(t) = -M_s\omega_{e,j}^2\xi_j(t) + M_s\omega_{c,j}^2\xi_{j-1}(t) + M_s\omega_{c,j+1}^2\xi_{j+1}(t), \quad j = 1, 2, ..., N-1 \quad (5c)$$

$$M_s\ddot{\xi}_N(t) = -M_s\Omega_N^2\xi_N(t) + M_s\omega_{c,N}^2\xi_{N-1}(t) - M_s\beta_{N+1}\dot{\xi}_N(t) + M_sf_{N+1}(t) \quad (5d)$$

In eq 5d, the adiabatic frequency $\Omega_N$ determines the long-time response of the heat bath, and the friction coefficient $\beta_{N+1}$ governs the dissipation of energy from the primary zone to the heat bath. The values of $\beta_{N+1}$ are very close to $\pi\omega_D/6$, where $\omega_D$ is the Debye frequency.[20] The Debye temperature of Si is 640 K.[23] These values and those of $\omega_e$'s, $\omega_c$'s, and $\Omega$'s are presented elsewhere.[24] The last term $M_sf_{N+1}(t)$ is the stochastic or random force on the primary system arising from thermal fluctuation in the heat bath and it balances, on average, the dissipative force $M_s\beta_{N+1}\dot{\xi}_N(t)$, which removes energy from the primary system in order that the equilibrium distribution of energies in the primary system be restored after collision.

The initial conditions needed to solve the equations of motion given by eq 4 and 5 are given in ref 18. The numerical procedures include the use of Monte Carlo routines to generate random numbers for the initial conditions. The first step is to sample collision energies $E$ from a Maxwell distribution at gas temperature $T_g$ and to weight the initial energy of H−Si and all chain atom vibrations by a Boltzmann distribution at surface temperature $T_s$. The normal component of the incident energy is then $E\cos^2\theta_{inc}$, which will be used in solving the equations of motion, where $\theta_{inc} = \tan^{-1}(\rho/z)$ and $z = Z - r_{HSi}\cos(\alpha + \theta)$. In sampling impact parameters, we take the flat range of $0 < b < b_{max}$, where $b_{max} = (3.057 + {}^1/_2 5.153)$ Å = 5.633 Å. Here 3.057 Å is the horizontal distance between the equilibrium position of H(ad) and the surface normal axis through third Si, 2.524 Å + 1.514 Å sin α, and 5.153 Å is the nearest Si−Si distance between two different strands (i.e., zeroth and seventh Si).[22] This wide range of $b$ will enable us to treat all trajectories, including those approaching the third Si from the left-hand side, important in the reaction. Also sampled are the initial values of $\theta$, $\phi$, and $\Phi$. Thus, each trajectory is generated with the set ($E$, $b$, $E^0_{HSi}$, $\theta_0$, $\phi_0$, $\Phi_0$, $\{\xi\}_{n0}$), where $E^0_{HSi}$ represents the initial energy of the HSi vibration, and $\{\xi\}_{n0}$ stands for the initial values of ($\xi_0$, $\xi_1$, ..., $\xi_N$)$_n$ for $n$ = 0−8. A typical number of trajectories used for each calculation is 30 000. We follow each trajectory for 50 ps, which is a sufficiently long time for OH(g) to recede from the influence of surface interaction, to confirm the occurrence of a reactive event forming OH. Furthermore, we confirm that each trajectory can be successfully back-integrated in the numerical procedure. We take the length $N$ = 9 for each chain.[16] That is, 9($N$ + 1) = 90 Si atoms are included

**TABLE 1: Potential and Spectroscopic Constants**

(a) O(g) + H(ad)/Si → OH(g) + Si

| interaction (i) | O−H | H−Si | O−surface |
|---|---|---|---|
| $D^0_{0,i}$ (eV)[a] | 4.392 | 3.50 | 3.82 |
| $\omega_i$ (cm$^{-1}$)[b] | 3738 | 2093 | 972 |
| $d_i$ (Å)[c] | 0.9697 | 1.514 | 1.709 |
| $a_i$ (Å)[d] | 0.2178 | 0.334 | 0.185 |

(b) O(g) + D(ad)/Si → OD(g) + Si

| interaction (i) | O−D | D-Si | O−surface |
|---|---|---|---|
| $D^0_{0,i}$ (eV)[a] | 4.453 | 3.50 | 3.82 |
| $\omega_i$ (cm$^{-1}$)[b] | 2720 | 1481 | 972 |
| $d_i$ (Å)[c] | 0.9697 | 1.514 | 1.709 |
| $a_i$ (Å)[d] | 0.2178 | 0.334 | 0.185 |

[a] $D_i = D^0_{0,i} + {}^1/_2\hbar\omega_i$ (ref 25 for O−H; refs 26 and 27 for H−Si; ref 28 for O−Si). [b] Reference 25 for O−H; refs 14 and 29 for H−Si; ref 28 for O−Si. Here the H−Si value 2093 cm$^{-1}$ is the $z$ direction vibrational frequency $\omega_{HSi,z}$. For the $x$ and $y$ directions, the vibrational frequencies are $\omega_{HSi,x} = \omega_{HSi,y} = 645$ cm$^{-1}$. The O−Si value 972 cm$^{-1}$ is the average of the observed values lying between 965 and 980 cm$^{-1}$ (refs 30 and 31). [c] Reference 25 for O−H; ref 22 for H−Si; ref 28 for O−Si. [d] $a_i = (D_i/2\mu_i)^{1/2}(1/\omega_i)$.

in the model. The pertinent potential and spectroscopic constants[14,25−31]used in the calculation are listed in Table 1.

## III. Results and Discussion

We first consider the probabilities of OH (OD) formation and amounts of energy deposited in the vibrational motion of OH (OD). Calculation of the energy deposited in OH (OD) from the computer output is straightforward. The translational energy is $E_{trans,OH} = {}^1/_2 m_{OH}(\dot{Z} - \gamma_H \cos\theta_{inc}\, \dot{r}_{OH})^2$, where $m_{OH} = (m_O + m_H)$ and $\gamma_H = m_H/(m_H + m_O)$. The rotational energy is $E_{rot,OH} = L_{OH}^2/2\mu_{OH}r_{OH}^2$, where $L_{OH}$ is the angular momentum $\mu_{OH}(z\dot{\rho} - \rho\dot{z})$ corresponding to the quantum number $J_{OH} = L_{OH}/\hbar$. The expression for the OH vibrational energy takes the usual form

$$E_{vib,OH} = {}^1/_2\mu_{OH}\dot{r}_{OH}^2 + D_{OH}[1 - e^{(r_{OH,e}-r_{OH})/2a}]^2 \qquad (6)$$

where $a$ is the interaction range parameter for the OH bond and $r_{OH,e}$ is the equilibrium value of $r_{OH}$. The expression for the energy propagated from the reaction zone into the solid bulk phase through the ($N$+1)-atom chain is[18]

$$E_{s,OH} = \sum_{i=0}^{8}[{}^1/_2 M_s \sum_{j=0}^{N}\dot{\xi}_j^2(t) + {}^1/_2 M_s \sum_{j=0}^{N-1}\omega_{e,j}^2\xi_j^2(t) + {}^1/_2 M_s\Omega_N^2\xi_N^2(t) + M_s\sum_{j=0}^{N-1}\omega_{c,j+1}^2\xi_j(t)\xi_{j+1}(t)]_i \qquad (7)$$

We average all these energies over the ensemble of reactive trajectories to obtain the quantities $\langle E_{trans,OH}\rangle$, $\langle E_{rot,OH}\rangle$, $\langle E_{vib,OH}\rangle$, and $\langle E_{s,OH}\rangle$ . We use similar expressions for O(g) + D(ad)/Si.

**A. Reaction Probabilities.** The reaction probability of the OH formation, O(g) + H(ad)/Si → OH(g) + Si, for the HSi vibration in the ground state is 0.106, which is calculated as the ratio of the number of reactive trajectories forming OH to the total number of trajectories sampled. As shown in Figure 3, the probability of OH formation increases linearly with increasing initial excitation of the HSi vibration. For example, when the initial HSi vibrational level is raised to the energy corresponding to the vibrational level $v_{HSi} = 3$, the probability of OH formation increases to 0.163. The dependence of the OH probability on the initial energy of the HSi vibration can best be represented by the linear equation $P_{OH} = 0.1022 + 0.0196v_{HSi}$. For the deuterated system, O(g) + D(ad)/Si → OD(g) + Si, the reaction probability $P_{OD}$ for $v_{DSi} = 0$ is 0.0940, which is somewhat smaller than $P_{OH}$, but for $v_{DSi} = 3$, it is only 0.115, which is significantly less than the corresponding $P_{OH}$. This result indicates that it is difficult for the incident atom to dislodge a heavier adatom from the surface and combine with it to form OD.

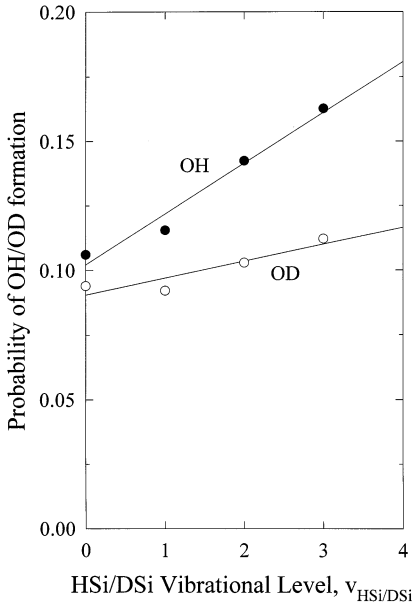


**Figure 3.** Probabilities of OH and OD formation as a function of the initial vibrational state of the adsorbate. The upper line is for the OH formation and the lower is for the OD formation.

The total reaction cross section calculated using the impact parameter-dependent probability function $P(b)$, the opacity function, in the expression $2\pi\int_0^{b_{max}} P(b)\, b\, db$ is 2.54 Å$^2$ for the OH formation reaction when $v_{HSi} = 0$. It rises to 4.45 Å$^2$ when $v_{HSi}$ is increased to 3. Similarly, for the deuterated reaction, the total reaction cross section of OD formation increases from 1.81 Å$^2$ at $v_{DSi} = 0$ to 2.63 Å$^2$ at $v_{DSi} = 3$, indicating that OD formation tends to occur at smaller impact parameters than in the OH case. Although the main goal of the present work is to study the OH (OD) formation, it is important to note that the major reaction in this collision system is the oxygen−hydrogen exchange reaction, O(g) + H(ad)/Si → O(ad)/Si + H(g), with reaction probability as large as 0.802 for $v_{HSi} = 0$. For this efficient pathway, the total reaction cross section is 92.0 Å$^2$, representing the dominance of large-$b$ collisions in which the incident atom strongly interacts with adjacent surface sites. The nearly identical value of 93.7 Å$^2$ is found for the deuterated system. Such an efficient atom−atom exchange reaction is also known to take place in the related reaction D(g) + H(ad)/Si → D(ad)/Si + H(g).[32]

In Figure 4, we show the dependence of the opacity function $P(b)$ on the impact parameter for the OH/OD formation. In each collision system, we consider HSi (DSi) initially to have vibrational energy corresponding to $v_{HSi} = 0$ or 3 (see Figure 4, parts a and b, for OH and Figure 4, parts c and d, for OD). This $b$ dependence provides useful information about the region where OH formation occurs. For the adatom−surface vibration initially in the ground state, the OH/OD formation occurs in small $b$ collisions ($0 < b < 1.5$ Å), where $P(b)$ rises rapidly from a small value at $b = 0$ to the maximum value of ≈0.6 at $b = 0.65$ Å for OH (see Figure 4a). For OD, the maximum occurs at smaller value of $b$ (Figure 4c), but the general variation of $P(b)$ on $b$ is similar to the OH case. Because the adatom is

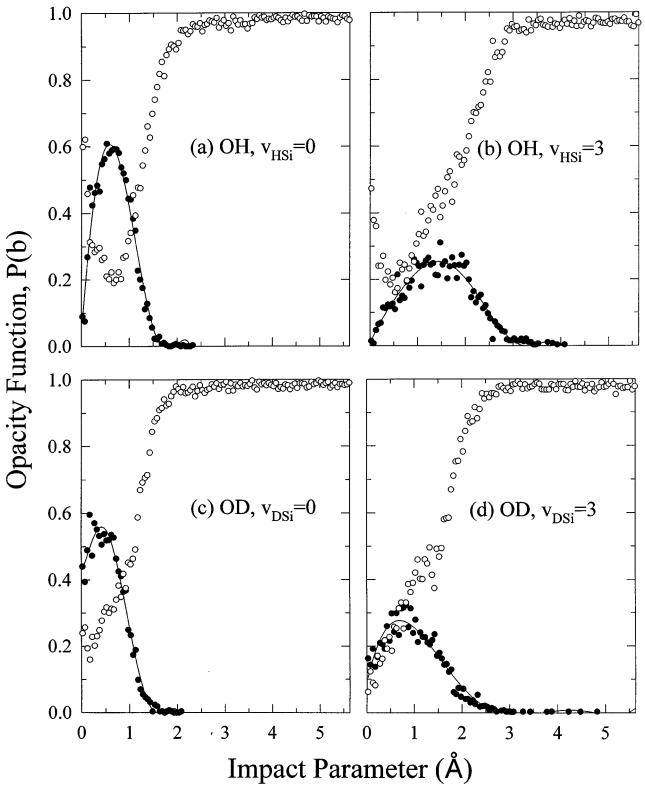


**Figure 4.** Dependence of the OH (OD) formation on the impact parameter for the initial vibrational state of the adsorbate 0 and 3 (filled circles). Parts a and b are for OH, and parts c and d are for OD. Also plotted for comparison is the *b* dependence of the opacity function for the O−H (O−D) exchange reaction (open circles).

tilted, the $b = 0$ collision in a three-dimensional collision does not represent the collinear configuration of O···H−Si. Therefore, the $b = 0$ collision is not the most efficient configuration for flow of energy between the loosely bound O···H bond and H−Si bond in the short-lived O···H−Si collision complex. The narrowness of the impact parameter range indicates that, especially for the $v_{HSi} = 0$ case, OH formation is localized in the neighborhood of the adatom site. Because the HSi bond is tilted, the incident atom hitting H(ad) head-on at $\theta_{inc} = 0$ is (1.514 Å)(sin 20.6°) = 0.533 Å away from the axis normal to the zeroth Si atom. Thus, for example, if we assume the O-to-H distance to be 0.97 Å, the normal OH bond distance, the three atom (O, H, Si) in the OH formation reaction can align almost collinearly in $\Phi = 0°$ direction when the incident atom reaches the distance where $b \approx 0.34$ Å. In the ±10% range of the normal OH bond distance, the collinear configuration occurs when the impact parameter lies in the range of 0.31−0.38 Å. In the OD case, the maximum of the opacity function shifts toward a smaller *b*. When $v_{HSi} = 3$, Figure 4b shows the OH probability maximum with a broad peak to be near $b = 1.5$ Å. A similar shift of the maximum toward a smaller *b* is seen for $v_{DSi} = 3$ in Figure 4d. In OD formation, a larger contribution comes from $b \approx 0$ collisions compared to the OH case.

For comparison, we plot the opacity function for the O−H exchange reaction O(g) + H(ad)/Si → O(ad)/Si + H(g) in Figure 4 (see open circles). It is very close to unity in large-*b* collisions ($b > 1.5$ Å for $v_{HSi/DSi} = 0$ and $b > 2.5$ Å for $v_{HSi/DSi} = 3$), where the incident atom approaches close to adjacent surface atoms. In the neighborhood of $b = 1.5$ or 2.5 Å, the opacity function for the OH (OD) formation and O−H (O−D) exchange reaction varies in opposite directions as the impact parameter changes. At the impact parameter below this value, the exchange reaction for HSi (DSi) initially in the ground state is less efficient

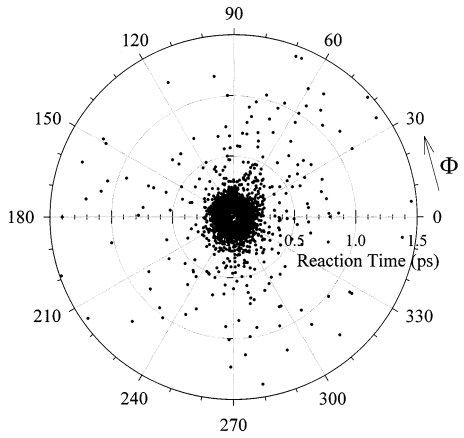


**Figure 5.** Distribution of reaction times. Plotted are reaction times of all OH forming events as a function of Φ. The $\Phi = 0°$ line measures the direction from zeroth Si to seventh Si, see Figure 1b.

because the incident atom has a greater tendency to react directly with the adatom. For HSi (DSi) initially in the excited state, both OH (OD) formation and O−H (O−D) exchange reactions are comparable in small-*b* collisions, especially in the OD case (see Figure 4, parts b and d). We note that in a small-*b* collision the exchange reaction tends to occur at the zeroth Si site (i.e., a direct exchange step), whereas in large-*b* collisions, the exchange step occurs when O(g) adsorbs on one of eight adjacent sites as H(ad) desorbs from the zeroth site, a concerted mechanism.

The formation of OH (OD) for HSi (DSi) initially in the ground state occurs in a small-*b* direct collision on a subpicosecond time scale. In Figure 5, we show the distribution of reaction times on the angle Φ, the azimuthal angle for O(g) on the surface plane. Reactive events are highly concentrated in the region of reaction times less than 0.3 ps. Such a short time scale supports the occurrence of OH formation in a direct collision-induced pathway via an Eley−Rideal (ER) mechanism. The distribution also shows no particular preference in the direction of approach of O(g) to the surface in producing a reactive event. Although its number is not large, there is an important group of reactive events, which occur at a much longer reaction time (≥1 ps). Such reactive events undergo a complex-mode collision, in which O(g) forms a loosely bound complex with the adatom for a lifetime of ≥1 ps before receding as OH-(g).

Before closing this section, we briefly comment on the fate of the remaining trajectories. For $v_{HSi} = 0$ in O(g) + H(ad)/Si, the probability of trapping the oxygen atom on an adjacent site without dissociating the adatom, i.e., O(g) + H(ad)/Si → O(ad)/Si + H(ad)/Si, is 0.0066. Another pathway is the collision-induced dissociation of the adatom without forming OH or causing adsorption of O, O(g) + H(ad)/Si → O(g) + H(g) + Si, for which the reaction probability is as small as 0.0008. In O(g) + D(ad)/Si, these two probabilities are 0.0062 and 0.0008, respectively, which are essentially identical to the former case. The trapping pathway is the outcome of the PES having a shallow attractive well in the entrance channel. When we attempt to remove the potential well by varying the Sato parameters from the chosen set (0.50, −0.05, 0.20, 0.50), there is a significant rise in the barrier height, thus making the OH (OD) formation inefficient. For (0.50, −0.05, 0.20, 0.45), the well depth is still 0.30 kcal/mol, but the barrier height rises to 1.15 kcal/mol. When the Sato parameter for the O-to-N = 0 Si atom is changed from 0.45 to 0.40 while holding all others unchanged in the previous set, the well depth reduces to 0.21 kcal/mol,

but the barrier height is now 2.55 kcal/mol. We note that, for (0.50, −0.05, 0.20, 0.30), the well disappears, but the barrier height is as high as 5.06 kcal/mol, which is too high for the present H-atom attraction reaction to occur. The variation of other Sato parameters produces a similar trend. For example, when we change the Sato parameter for the H−Si interaction from −0.05 to −0.15 to the above-mentioned $\Delta_{OS} = 0.40$ case such that the (0.50, −0.15, 0.20, 0.40), the well depth is 0.14 kcal/mol, but the barrier height is as high as 3.24 kcal/mol. The set (0.50, −0.05, 0.20, 0.50) used in the present study has been selected after systematically varying the values of Δ's within a physically reasonable range.

**B. Dependence of OH Formation on Surface Temperature.** Dependence of the OH formation on the surface temperature is not very strong. The probabilities for HSi initially in the ground state at $T_s = 0$, 300, and 600 K, with the gas temperature fixed at 1500 K, are 0.087, 0.107, and 0.111, respectively, a weak temperature dependence which is characteristic of the ER mechanism. For OD formation with $v_{DSi} = 0$, the probabilities are 0.085, 0.094, and 0.098, respectively, at the corresponding surface temperatures. Thus, OD formation, which involves the dissociation of a heavier atom from the surface, is less efficient than OH formation. The difference is negligible at 0 K, but it is about 10% at the higher temperatures.

The results of the present calculation can be compared with other studies on related gas−surface reaction.[13] The variation of the probability of OH formation with increasing surface temperature and initial excitation of the adatom−surface vibration in the present study is similar to that of the ER-type hydrogen recombination on a silicon surface. For H(g) +H-(ad)/Si, the adatom−surface bond is the same as that in the present study and the H-to-H interaction energy $D_0^0 = 4.478$ eV[25] is very close to the present O-to-H interaction energy $D_0^0 = 4.392$ eV. In the present study, the ratio of the OH formation probability at $T_s = 600$ K to that at 300 K for $v_{HSi} = 0$ is 0.111/0.106 = 1.05, which compares well with the ratio of 0.112/0.109 = 1.03 for the reaction H(g) + H(ad)/Si → $H_2$(g) + Si.[13] Here we assumed the HSi vibration to be at surface temperature 300 K. Because the vibrational quantum of HSi is 0.259 eV, the fraction of HSi in excited vibrational states is only $4.36 \times 10^{-5}$ at 300 K. Even if the vibrational motion maintains the gas temperature of 1500 K, the fraction of HSi vibration in the ground state is still as large as 0.866. Thus, the contribution from initially excited vibrational states to the net probability in the present system is not important. It should be noted that, in ref 13, the incident atom energy is 0.030 eV, but we have used incident energies determined from the Maxwellian sampling at $T_g = 1500$ K. Because the reaction exothermicity is largely determined by the bond energies given above, however, the two reaction systems are energetically similar. In O(g) + D(ad)/Si with $v_{DSi} = 0$, the ratio of the probability at $T_s = 600$ K to that at 300 K is 0.0979/0.0936 = 1.05, compared with the ratio of 0.062/0.057 = 1.09 for the H(g) + D(ad)/Si reaction studied in ref 13. Another comparison is the dependence of the probability of OH formation on the initial state of the adsorbate vibration. Raising the initial vibrational state of the adsorbate from $v_{HSi} = 0$ to 1 increases the probability of OH formation in the present reaction from 0.106 to 0.116, an increase by ≈10%, as a result of increased energy in the reaction coordinate. The probability increases to 0.142 and 0.163 when the initial vibrational state is raised to $v_{HSi} = 2$ and 3. For H(g) + H(ad)/Si, also at $T_s = 300$ K but $E = 0.030$ eV, the probability ratio for $v_{HSi} = 1$ to 0 is known to be 0.182/0.109 = 1.67.[13] For two different reactions with similar reaction energetics, the effect of the initial vibrational state of the adsorbate on the gas−surface recombination reaction is qualitatively similar.

**TABLE 2: Distribution of the Reaction Exothermicity at 1500 and 300 K[a]**

(a) O(g) + H(ad)/Si → OH(g) + Si

| $v_{HSi}$ | $\langle E_{vib,OH}\rangle$ | $\langle E_{rot,OH}\rangle$ | $\langle E_{trans,OH}\rangle$ | $\langle E_{s,OH}\rangle$ |
|---|---|---|---|---|
| 0 | 0.378 | 0.145 | 0.367 | 0.130 |
| 1 | 0.566 | 0.142 | 0.388 | 0.109 |
| 2 | 0.745 | 0.168 | 0.384 | 0.103 |
| 3 | 0.941 | 0.199 | 0.378 | 0.106 |

(b) O(g) + D(ad)/Si → OD(g) + Si

| $v_{DSi}$ | $\langle E_{vib,OD}\rangle$ | $\langle E_{rot,OD}\rangle$ | $\langle E_{trans,OD}\rangle$ | $\langle E_{s,OD}\rangle$ |
|---|---|---|---|---|
| 0 | 0.373 | 0.188 | 0.340 | 0.103 |
| 1 | 0.525 | 0.187 | 0.361 | 0.095 |
| 2 | 0.670 | 0.184 | 0.356 | 0.093 |
| 3 | 0.789 | 0.189 | 0.363 | 0.097 |

[a] The ensemble-averaged energies are in eV.

**C. Product Energy Distribution.** The energy available for OH and the surface in O(g) + H(ad)/Si is $(\Delta D_0^0 + E_{HSi}^0 + E)$, where $E_{HSi}^0$ is the initial energy of the adatom−surface vibration and $E$ is the oxygen atom kinetic energy. The reaction exothermicity $\Delta D_0^0$ is the difference between the HSi dissociation energy and OH dissociation energy. From the dissociation energies listed in Table 1, we find $\Delta D_0^0 = 0.892$ eV for this exothermic reaction, which is characterized by an attractive PES shown in Figure 2. In Table 2, we summarize the ensemble-averaged values of energies deposited in the translational, rotational and vibrational motions of OH (OD) as well as that propagated into the solid for $v_{HSi}(v_{DSi}) = 0$, 1, 2, and 3. For $v_{HSi} = 0$, the energies deposited in the translational, rotational and vibrational motions of OH in O(g) + H(ad)/Si → OH(g) + Si are $\langle E_{trans,OH}\rangle = 0.367$, $\langle E_{rot,OH}\rangle = 0.145$, and $\langle E_{vib,OH}\rangle = 0.378$ eV. The amount of energy propagated into the solid in this reaction is $\langle E_{s,OH}\rangle = 0.130$ eV. Here we use the notation with OH, i.e., $\langle E_{s,OH}\rangle$, simply to signify energy propagation to the solid in the OH forming reaction. Thus, the gas-phase product OH carries away the majority of the reaction exothermicity. In particular, nearly 75% of the reaction energy is deposited in the vibrational and translational motions. This type of product energy distribution with a major portion depositing in translation and vibration is characteristic of an ER mechanism.[15,33] Only about 13% of the reaction energy is propagated into the bulk solid phase. Increasing the initial vibrational state of the adsorbate vibration from $v_{HSi} = 0$ to 1, 2, and 3 changes the OH translational energy, as well as the surface energy, only slightly. However, we did find a large increase in the vibrational energy with increasing $v_{HSi}$, indicating the occurrence of strong product vibrational excitation. The combined effect of a weak dependence of $\langle E_{s,OH}\rangle$ and strong dependence of $\langle E_{vib,OH}\rangle$ on $v_{HSi}$ is interesting, because it indicates that the additional energy resulting from initial H−Si vibrational excitation preferentially flows toward the O···H bond in the short-lived O···H−Si complex and eventually deposits in the vibration. In the O(g) + D(ad)/Si reaction, where a heavier adatom is involved, the dependence of $\langle E_{trans,OD}\rangle$ and $\langle E_{s,OD}\rangle$, even including $\langle E_{rot,OD}\rangle$, on $v_{DSi}$ is particularly weak. The $v_{DSi}$ dependence of $\langle E_{vib,OD}\rangle$ is very similar to the OH case.

The vibrational energy-to-impact parameter relation for all OH forming events plotted in Figure 6 shows a gradual increase of the vibrational energy of OH as the initial vibrational excitation of HSi expressed by $v_{HSi}$, increases. Reactive events are bound between $b = 0$ and ≈2 Å, but the upper bound increases toward ≈3 Å as the initial excitation increases. In

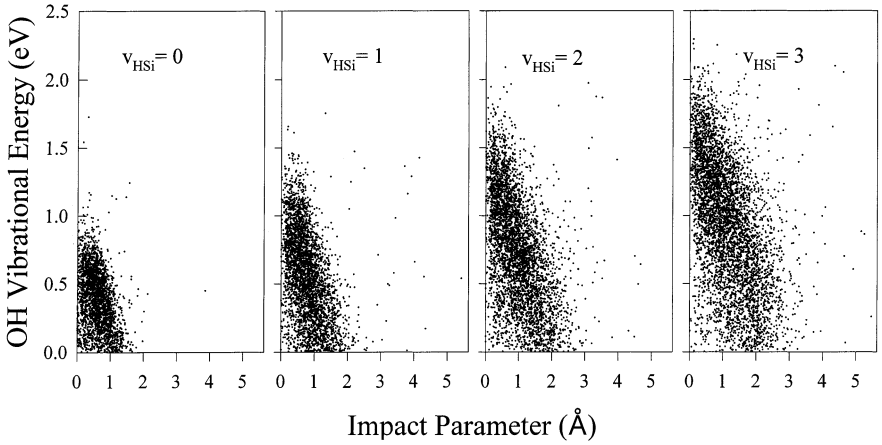


**Figure 6.** Distribution of the OH vibrational energy as a function of the impact parameter for the initial vibrational states of the adsorbate from $v_{HSi} = 0$ to 3.

particular, the events become concentrated at higher vibrational energies and smaller impact parameters as $v_{HSi}$ increases. The dominance of such small-*b* collisions leads to OH rotation sharing a smaller amount of the reaction energy. Although it is not shown, we find a very similar distribution of the four energies for the OD case.

When the initial vibrational state of the adsorbate is raised from $v_{HSi} = 0$ to 1, corresponding to the increase of initial vibrational energy by 0.256 eV, the ensemble-averaged energy deposited in the OH vibration increases from $\langle E_{vib,OH} \rangle = 0.378$ to 0.566 eV, an increase of 0.179 eV, whereas the energies of other motions change slightly as noted above. A similar increase is seen when $v_{HSi}$ rises from 1 to 2 and 2 to 3. There are other sources of energy, which can contribute to the newly formed OH bond, but the main contributor to the vibrational energy of OH is HSi through the V → V energy transfer pathway. Thus, nearly three-quarters of the energy initially deposited in the HSi vibration transfers to the nascent OH vibration. This efficient flow of energy occurs at close range during O(g)-to-H(ad)/Si interaction. At this range where the incident oxygen atom moves along the reaction coordinate, it becomes loosely bound to the adatom, forming a short-lived collision complex (O···H−Si), in which "intramolecular" VV coupling occurs. This coupling promotes the asymmetric stretching vibration of the three-atom configuration causing the O···H bond to strengthen as the H−Si bond weakens in a concerted mechanism. As the reaction progresses in the complex state, the vibrational motion of O···H starts with low frequency and increases toward the final OH frequency ($\omega_e = 3738$ cm$^{-1}$)[25] passing through the vibrational frequency of the H−Si bond ($\omega_e = 2093$ cm$^{-1}$).[26] Near and at this frequency, "intramolecular" flow of vibrational energy from H−Si to O···H, the V → V process, takes place efficiently. Such near-resonant or resonant energy transfer is known to be the principal energy flow pathway in molecular collisions, ranging from intermolecular diatom−diatom collisions to intramolecular processes in polyatomic molecules.[34,35] We note that the incident atom carries a significant amount of the collision energy, but its transfer to the nascent vibration is not efficient, i.e., a collision-induced T → V energy transfer process in this gas−surface reaction is inefficient.

The dependence of the ensemble-averaged vibrational energy $\langle E_{vib,OD} \rangle$ on the initial state of adatom−surface vibration is very similar to the OH case. We find a large portion of the D−Si vibrational energy transferring to the O···D bond during the brief residency of O(g) on the adatom in the O···D−Si configuration.

We can recast the results present in Figure 6 in the vibrational population as shown in Figure 7, where the population distribution is prepared by assigning the quantum number $v_{OH}$ determined as $v_{OH} = \text{int}[E_{vib,OH}/E_{vib}(v_{OH})]$, the integer nearest to the ratio $E_{vib,OH}/E_{vib}(v_{OH})$. Here $E_{vib}(v_{OH})$ is the vibrational energy determined from the eigenvalue expression $E_{vib}(v_{OH}) = \omega_e(v + {}^1/_2) - \omega_e x_e(v + {}^1/_2)^2$ with $\omega_e = 3737.76$ cm$^{-1}$ and $\omega_e x_e = 84.881$ cm$^{-1}$.[25] For the initial vibrational energy of HSi corresponding to $v_{HSi} = 0$, the intensity of the vibrational population for the $v_{OH} = 1$ level is as large as 0.340 compared with 0.637 for $v_{OH} = 0$, which represents the occurrence of a strong vibrational excitation (see Figure 7a). At gas temperature 1500 K, the Boltzmann distribution gives the fractions $f(v_{OH} = 0) = 1 - e^{-\hbar\omega/kT} = 0.972$ and $f(v_{OH} = 1) = (1 - e^{-\hbar\omega/kT})e^{-\hbar\omega/kT} = 0.027$, so the ratio $f(v_{OH} = 1)/f(v_{OH} = 0)$ is only 0.028; thus, the present result shown in Figure 7a giving $f(v_{OH} = 1)/f(v_{OH} = 0) = 0.534$ seriously deviates from the prediction of the Boltzmann distribution law. The deviation becomes even larger when $v_{HSi}$ is raised. For example, for $v_{HSi} = 1$ shown in Figure 7b, the population intensity of $v_{OH} = 1$ is now greater than that of $v_{OH} = 0$, a population inversion.[12,36] As shown in Figure 7, parts c and d, the inversion becomes stronger as we raise the initial excitation to the $v_{HSi} = 2$ and 3 states. For $v_{HSi} = 3$, the intensities are 0.180, 0.265, 0.307, and 0.196 for $v_{OH} = 0$, 1, 2, and 3, respectively (see Figure 7d). For this initial excitation, we find OH forming even in an excited state as high as $v_{OH} = 5$, although the population intensity is only 0.0035 (not shown in Figure 7d). The vibrational population distributions for OD shown in Figure 7e−h are similar to those of the OH case. In O(g) + D(ad)/Si, where the vibrational energy levels of DSi are narrower than those of HSi, the extent of vibrational excitation is larger. For $v_{DSi} = 0$, $f(v_{OD} = 1)/f(v_{OD} = 0) = 0.826$, which is significantly larger than 0.534 in the OH case. The high vibrational excitation of OH (OD) reported here is characteristic of the ER mechanism. In the Langmuir−Hinshelwood mechanism, where the product molecules thermally equilibrate with the surface before desorbing, vibrational excitation is generally not significant.

Before closing this section, we briefly comment on the dependence of product energy distributions on the surface temperature; see Table 3. Here the gas temperature is fixed at 1500 K as in Table 2 and the values for $T_s = 300$ K are reproduced from Table 2. The principal qualitative feature of the data is the weak temperature dependence for all cases considered. That is, the variation of surface temperature is of little consequence in determining the energies of gas-phase

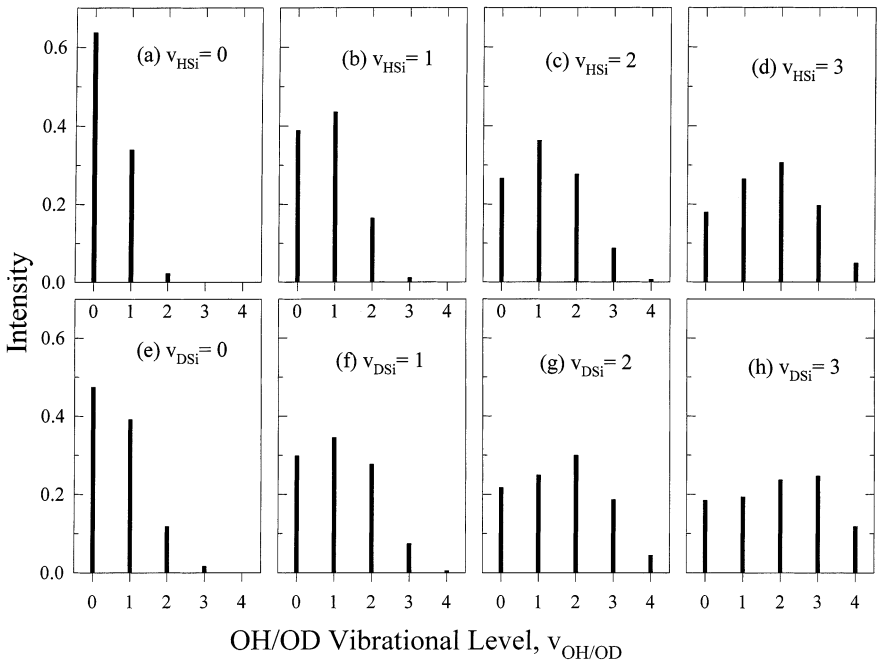


**Figure 7.** OH (OD) vibrational population distribution. The upper four graphs (a−d) are for OH, and lower four graphs (e−h) are for OD.

**TABLE 3: Dependence of the Product Energy Distribution on the Surface Temperature**[a]

(a) O(g) + H(ad)/Si → OH(g) + Si; $v_{HSi} = 0$

| $T_s$ (K) | $\langle E_{vib,OH}\rangle$ | $\langle E_{rot,O}H\rangle$ | $\langle E_{trans,OH}\rangle$ | $\langle E_{s,OH}\rangle$ |
|---|---|---|---|---|
| 0 | 0.371 | 0.153 | 0.358 | 0.118 |
| 300 | 0.378 | 0.145 | 0.367 | 0.130 |
| 600 | 0.381 | 0.141 | 0.379 | 0.141 |

(b) O(g) + D(ad)/Si → OD(g) + Si; $v_{DSi} = 0$

| $T_s$ (K) | $\langle E_{vib,OD}\rangle$ | $\langle E_{rot,OD}\rangle$ | $\langle E_{trans,OD}\rangle$ | $\langle E_{s,OD}\rangle$ |
|---|---|---|---|---|
| 0 | 0.397 | 0.177 | 0.364 | 0.112 |
| 300 | 0.373 | 0.188 | 0.340 | 0.103 |
| 600 | 0.395 | 0.187 | 0.341 | 0.105 |

[a] The gas temperature is maintained at 1500 K. Ensemble-averaged energies are in eV.

product OH (OD). Furthermore, the energy propagated into the bulk surface is essentially independent of $T_s$ for the OD case, in which the adsorbate atom is heavier, although the dependence is somewhat significant in the OH case. In the latter case, $\langle E_s$,-OH$\rangle$ increases from 0.118 eV at $T_s = 0$ K to 0.130 eV at $T_s =$ 300 K and then to 0.141 eV at $T_s = 600$ K.

**D. Tunneling Effects.** In the H abstraction reaction, a correction for reaction coordinate motion must be included to account for tunneling effects. The dissociating H can combine with the oxygen atom by tunneling through the barrier. To correct for tunneling, we use the WKB expression for the probability of tunneling through the barrier given by[37]

$$G(E_H) = \exp[-(2/\hbar)\int_{R_1}^{R_2}\{2m_H[V(R) - E_H]\}^{1/2}\,dR] \quad (8)$$

where $V(R)$ is the potential energy barrier function along the reaction path determined numerically from the computed LEPS−PES given in Figure 2b, and $R_1$ and $R_2$ define the width of the barrier at the kinetic energy of dissociating H, $V(R) = E_H$, the kinetic energy of H. For convenience, we have chosen the direction of reaction from left to right so the reaction coordinate varies from negative to positive with respect to the barrier, which is taken to be the origin of the plot; i.e., $R = 0$ (see Figure 8, parts a and b). Also shown in Figure 8a are the

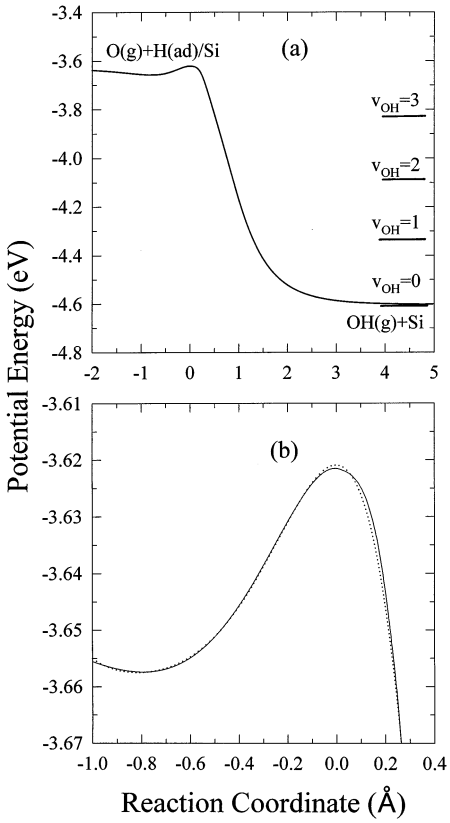


**Figure 8.** (a) Potential energy profile along the reaction coordinate for O···H−Si based on the potential energy surface given in Figure 2. Also shown are the energetically accessible vibrational levels of OH product at the threshold. (b) Potential energy profile in the barrier region. The dotted curve is the best fit to the calculated value (see the text).

energetically accessible vibrational levels of product OH at the threshold. This profile is very similar to a well-known exothermic reaction F + $H_2$ → HF + H.[38] For the incident atom approaching the surface from infinity, the portion of the product-side potential profile measured below the potential minimum has no effect on tunneling. The best-fit function to the potential energy in the barrier region including the entrance level shown

in Figure 8b is the polynomial $V(R) = -3.6210 - 0.001536R - 0.4075R^2 - 0.8835R^3 - 0.7526R^4 - 0.2410R^5$ in eV.

The tunneling correction is the Maxwell-Boltzmann average of eq 8[39−41]

$$\Gamma(T) = \frac{e^{-V_o/kT}}{\hbar}\int_0^\infty G(E_H)e^{-E_H/kT}\,dE_H \qquad (9)$$

where $V_o$ is the barrier height. Because H is adsorbed on the surface, which is maintained at 300 K, it is reasonable to evaluate the tunneling correction at this temperature. The numerical evaluation of eq 9 for $G(E_H)$ at 300 K is 0.0437 for OH and 0.0290 for OD. Because the barrier height is low, the temperature dependence of $\Gamma(T)$ is not expected to be significant. For example, at temperature as high as the gas-phase value of 1500 K, $\Gamma(T)$ values for OH and OD formation slightly increase to 0.0510 and 0.0363, respectively. Thus, the quantum tunneling effect can increase the probability of OH (OD) formation calculated in the classical trajectory procedure by a few percent at most with a larger effect on the lighter-atom system.

## IV. Concluding Comments

Calculations of the O(g) + H(ad)/Si reaction using classical trajectory procedures show a modest extent of OH (OD) formation. The incident gas atom is modeled to interact with the adatom on the surface composed of 90 Si atoms of nine 10-atom chains. The end atom of each chain is coupled to the bulk phase. At gas temperature 1500 K and surface temperature 300 K, about 10% of the total trajectories sampled lead to OH (OD) formation. The product OH (OD) is ejected from the surface on a subpicosecond time scale in a small impact-parameter collision before thermal equilibration can occur. A major portion of the reaction exothermicity deposits in the vibrational and translational motions of OH (OD), whereas a much smaller amount transfers to the rotational motion. The amount of energy propagated into the surface is only about 10% of the available energy. The dependence of the probability of OH formation and product energy distribution on the surface temperature between 0 and 600 K is found to be weak.

The energy initially stored in the adatom−surface vibration preferentially transfers to the vibrational motion of OH (OD), representing an efficient intramolecular vibration-to-vibration energy flow in the short-lived collision complex O···H−Si or O···D−Si on the surface. Thus, the amount of energy deposited in the product vibration varies strongly with the initial vibrational state of the adsorbate. Such dependence is absent in the energies of all other motions including the energy transferred to the surface. Vibrational population does not follow the Boltzmann distribution, exhibiting a population inversion. The inversion becomes particularly strong when the initial vibrational energy of the adsorbate increases.

When the effect of barrier penetration of H is included, the probability of OH formation increases by about 4% over the classical trajectory result. The increase in OD formation is about 3%.

**Acknowledgment.** J.R. gratefully acknowledges the Korean Research Foundation for financial support. Y.H.K. gratefully acknowledges Inha University and 21st Century Korean Foundation for financial support.

## References and Notes

(1) Shustorovish, E. *Surf. Sci. Rep*. **1986**, *6*, 1.
(2) Christmann, K. *Surf. Sci Rep*. **1988**, *9*, 1.
(3) Weast, R. C., Ed.; *CRC Handbook of Chemistry and Physics*, 64th ed.; CRC Press: Boca Raton, FL, 1983; pp F176−F181.
(4) Hall, R. I.; Cadez, I.; Landau, M.; Pichou, F.; Schermann, C. *Phys. Rev. Lett.* **1988**, *60*, 337.
(5) Eenshuistra, P. J.; Bonnie, J. H. M.; Lois, J.; Hopman, H. *Phys. Rev. Lett.* **1988**, *60*, 341.
(6) Kratzer, P.; Brenig, W. *Surf. Sci*. **1991**, *254*, 275
(7) Jackson, B.; Persson, M. *Surf. Sci*. **1992**, *269*, 195.
(8) Schermann, C.; Pichou, F.; Landau, M.; Cadez, I.; Hall, R. I. *J. Chem. Phys*. **1994**, *101*, 8152.
(9) Weinberg, W. H. In *Dynamics of Gas−Surface Interaction*; Rettner, C. T., Ashfold, M. N. R., Eds.; Royal Society of Chemistry, Thomas Graham House: Cambridge, England, 1991; pp 171−219.
(10) Jackson, B.; Persson, M. *Surf. Sci*. **1992**, *269*, 195.
(11) Ree, J.; Kim, Y. H.; Shin, H. K. *J. Phys. Chem. A* **1997**, *101*, 4523.
(12) Shin, H. K. *J. Phys. Chem. A* **1998**, *102*, 2372.
(13) Koleske, D. D.; Gates, S. M.; Jackson, B. *J. Chem. Phys*. **1994**, *101*, 3301.
(14) Kratzer, P. *J. Chem. Phys*. **1997**, *106*, 6752.
(15) Buntin, S. A. *J. Chem. Phys*. **1998**, *108*, 1601.
(16) Ree, J.; Shin, H. K. *J. Chem. Phys*. **1999**, *111*, 10261.
(17) Ree, J.; Kim, Y. H.; Shin, H. K. *Chem. Phys. Lett*. **2002**, *353*, 368.
(18) Kim, Y. H.; Ree, J.; Shin, H. K. *J. Chem. Phys*. **1998**, *108*, 9821.
(19) Kim, W. K.; Ree, J.; Shin, H. K. *J. Phys. Chem. A* **1999**, *103*, 411.
(20) Adelman, S. A. *J. Chem. Phys*. **1979**, *71*, 4471.
(21) McDowell, H. K. *J. Chem. Phys*. **2000**, *112*, 6971.
(22) Radeke, M. R.; Carter, E. A. *Phys. Rev*. **1996**, *B54*, 11803.
(23) Gray, D. E., Ed.; *American Institute of Physics Handbook*, 3rd ed.; McGraw-Hill: New York, 1972; p 4−116.
(24) Ree, J.; Kim, Y. H.; Shin, H. K. *J. Chem. Phys*. **1996**, *104*, 742.
(25) Huber, K. P.; Herzberg, G. *Constants of Diatomic Molecules*; Van Nostrand Reinhold: New York, 1979.
(26) Van de Walle, C. G.; Street, R. A. *Phys. Rev*. **1995**, *B51*, 10615.
(27) Kratzer, P.; Hammer, B.; Norskov, J. K. *Phys. Rev*. **1995**, *B51*, 13432.
(28) Jenichen, A.; Johansen, H. *Surf. Sci*. **1988**, *203*, 143.
(29) Tully, J. C.; Chabal, Y. J.; Raghavachari, K.; Bowman, J. M.; Lucchese, R. R. *Phys. Rev*. **1985**, *B31*, 1184.
(30) Huffman, M.; McMillan, P. *J. Non-Cryst. Solids* **1985**, *76*, 369.
(31) Krol, J. M.; Rabinovich, E. M. *J. Non-Cryst. Solids* **1986**, *82*, 143.
(32) Lee, S. S.; Kong, M. J.; Bent, S. F.; Chiang, C. M.; Gates, S. M. *J. Phys. Chem*. **1996**, *100*, 20015.
(33) Gross, A. *Surf. Sci. Rep*. **1998**, *32*, 291.
(34) Yardley, J. T. *Introduction to Molecular Energy Transfer*; Academic: New York, 1980; Chapter 5.
(35) Shin, H. K. *J. Phys. Chem. A* **2000**, *104*, 6699.
(36) Kori, M.; Halpern, B. L. *Chem. Phys. Lett*. **1984**, *110*, 223.
(37) Landau, L. D.; Lifshitz, E. M. *Quantum Mechanics*; Addison-Wesley: Reading, MA, 1958; pp 171−175.
(38) Muckerman, J. T. *J. Chem. Phys*. **1971**, *54*, 1155.
(39) Johnston, H. S.; Heicklen, J. *J. Phys. Chem*. **1961**, *66*, 532.
(40) Shin, H. K. *J. Chem. Phys*. **1963**, *39*, 2934.
(41) Johnston, H. S. *Gas-Phase Reaction Rate Theory*; Ronald: New York, 1966; pp 38−47.